Simulating Dynamic Ultrasound Using MR-derived Motion Models to Assess Respiratory Synchronisation for Image-Guided Liver Interventions

Erik-Jan Rijkhorst, Daniel Heanes, Freddy Odille, David Hawkes, and Dean Barratt

Centre for Medical Image Computing, Department of Medical Physics and Bioengineering, University College London, London, United Kingdom
{e.rijkhorst,d.heanes,f.odille,d.hawkes,d.barratt}@ucl.ac.uk
http://cmic.cs.ucl.ac.uk

Abstract. Tracked intra-operative ultrasound can be registered to real-time synthetic ultrasound derived from a motion model to align pre-operative images with a patient's anatomy during an intervention. Furthermore, synchronisation of the motion model with the patient's breathing can be achieved by comparing diaphragm motion obtained from the tracked ultrasound, with that obtained from the synthetic ultrasound. The purpose of this study was to assess the effects of spatial misalignment between the tracked and synthetic ultrasound images on synchronisation accuracy. Deformable image registration of 4-D volunteer MR data was used to build realistic subject-specific liver motion models. Displacements predicted by the motion model were applied to acoustic parameter maps obtained from segmented breath-hold MR volumes, and dynamic B-mode ultrasound images were simulated using a fast ultrasound propagation method. To prevent synchronisation errors due to breathing variations between motion model acquisition and interventional ultrasound imaging from influencing the results, we simulated both the synthetic and the tracked ultrasound using a single motion model. Spatial misalignments of up to ± 2 cm between the tracked and synthetic ultrasound resulted in a maximum motion model breathing phase error of approx. 3 %, indicating that respiratory synchronisation of a motion model using tracked ultrasound is relatively insensitive to spatial misalignments.

Keywords: dynamic ultrasound, motion models, synchronisation, breathing, image guidance.

1 Introduction

Minimally- and non-invasive liver interventions, such as radio-frequency ablation and high-intensity focused ultrasound, rely on accurate image guidance to compensate for intra-operative respiratory motion. Over the past few years, several

N. Navab and P. Jannin (Eds.): IPCAI 2010, LNCS 6135, pp. 113–123, 2010.

methods for quantifying organ motion using 4-D CT or MR based motion models have been presented [1–4]. Such models can be used in combination with intra-operative imaging, such as B-mode ultrasound, to spatially align pre-operative images to the patient's anatomy during an intervention [5–8], allowing for a more accurate treatment of a target region.

Apart from spatial registration, accurate real-time temporal synchronisation of a motion model with the patient's breathing is equally important [4, 9]. To achieve this, a surrogate breathing signal needs to be available during intervention, for example by tracking skin markers [1] or using a navigator to track diaphragm motion [2, 4, 10].

The purpose of this study was to assess the effects on synchronisation accuracy of a pre-operative motion model with a subject's breathing due to spatial misalignment between tracked interventional ultrasound and real-time synthetic ultrasound derived from the motion model. Deformable image registration of free-breathing volunteer MR data was used to build a subject-specific liver motion model as a function of breathing phase. To obtain acoustic parameter maps, breath-hold MR volumes were segmented into liver, blood, lung, and ribs. The maps were deformed by applying the displacements predicted by the motion model, and a fast ultrasound propagation simulation was used to compute dynamic B-mode ultrasound images. One such simulated ultrasound sequence was used to represent the tracked ultrasound, while a second sequence, computed at a slightly different location to simulate spatial misalignment, represented the real-time synthetic ultrasound. A navigator window was positioned at the diaphragm in both simulated sequences, from which surrogate breathing signals and a motion model phase error were computed.

2 Materials and Methods

We propose the following scenario for synchronising a motion model to a subject's breathing during an intervention (Fig. 1). Prior to intervention, real-time

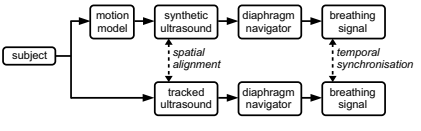

Fig. 1. Scenario for synchronising a motion model to a subject's breathing. Note that in this study both the tracked and synthetic ultrasound were simulated using a single motion model.

MR images are acquired and deformable image registration is used to obtain a motion model. High-resolution breath-hold MR images are segmented into different tissue types to allow the computation of simulated ultrasound images.

During intervention, tracked dynamic B-mode ultrasound images of the moving diaphragm are continuously acquired. Using the tracking information, these

images can be aligned spatially with the motion model co-ordinate system. A fast ultrasound simulation technique produces a synthetic dynamic B-mode sequence at the tracked location of the real ultrasound. These can be registered to the tracked ultrasound to improve spatial alignment between the motion model and the subject [5, 8]. Furthermore, by placing navigator windows at the moving diaphragm in both the tracked and synthetic ultrasound sequences, two breathing signals can be obtained, which may be used to synchronise the motion model with the breathing.

In this paper, assuming this scenario, we computed a synchronisation error measure due to spatial misalignment between the tracked and synthetic ultrasound. Instead of using real tracked ultrasound, we simulated it using the motion model in the same way as was done for the synthetic ultrasound. This prevented introducing additional synchronisation errors due to variations in a subject's breathing which may occur between motion model acquisition and interventional ultrasound imaging, and which are of potentially larger magnitude than the synchronisation errors due to misalignment. Furthermore, the breathing signal obtained from the simulated tracked ultrasound acts as a "ground-truth", which would not be available if real tracked ultrasound would have been used. The following sections present the different parts of our computations in more detail.

2.1 MR Data Acquisition

Data were acquired for three healthy volunteers using a 1.5 T cylindrical bore Philips Achieva MR scanner at Guy's Hospital, London. A fast 3-D T1-weighted gradient echo sequence (THRIVE) was used to obtain high-resolution scans during breath-hold, and 4-D (3-D+time) real-time scans during free breathing. Parallel imaging with a 32-channel coil array using a SENSE acceleration factor of 8 resulted in scan times of approx. 16 seconds per breath-hold volume, and 1 second per real-time volume, respectively. A respiratory signal, obtained from a pneumatic bellow placed around the chest of each volunteer, was recorded during all scans.

The breath-hold scans were acquired at exhale with a voxel size of $1.4 \times 1.4 \times 1.7$ mm^3 and a field-of-view of $400 \times 400 \times 270$ mm^3 covering the whole abdomen. To reduce the time needed for a single real-time scan, the sequence parameters were modified to decrease the spatial resolution to $1.5 \times 1.5 \times 4$ mm^3, while keeping a similar FOV. A total of $N^{\mathrm{acq}} = 40$ volumes were acquired over approx. 10 breathing cycles.

2.2 Deformable Registration of Real-Time Free Breathing Scans

To obtain a measure of breathing induced displacements throughout the liver, the real-time MR scans were registered using a non-rigid fluid registration method [11]. This method solves the time-dependent Navier-Lamé equations for a compressible viscous fluid resulting in a diffeomorphic transformation between source and target images. The registration is driven by image-derived forces and employs a full multi-grid scheme [11].

First, the real-time volume with a breathing phase closest to exhale was manually selected and used as the source (i.e reference) volume. This scan was registered to all other target volumes, resulting in a set of N^{acq} displacement fields for each volunteer.

To assess the registration accuracy, corresponding anatomical landmarks, including vessel bifurcations and points on the diaphragm, were picked manually in each volume, resulting in a set of N^{acq} points for each location. Landmark points were identified for each volunteer at five different locations distributed throughout the liver. The mean target registration error (TRE), defined as the mean of the Euclidean distance between each landmark point in the reference volume and corresponding points in the other volumes, was computed before and after registration.

2.3 Motion Model Breathing Phase from Respiratory Bellow Signal

To fit a motion-model to the registration results, the tissue displacement at each voxel must be known as a function of the breathing cycle. Since we would like to represent an average breathing cycle by sorting the sparse real-time data, and the amplitude of the bellow signal may vary across breathing cycles (see Fig. 2), we used the breathing phase instead [1, 12].

To compute the breathing phase from the bellow signal, it was first convolved with a Gaussian to obtain a signal with clearly defined minima at times $t_i^{\min}$, and maxima at times $t_i^{\max}$, $i = 1, ..., N^{\max}$. The minima were assigned a breathing phase of zero, while the phase of each maximum was set to the average phase over all maxima, $\bar{\phi}^{\max}$, calculated using

$$\bar{\phi}^{\max} = \frac{1}{N^{\max}} \sum_{i=1}^{N^{\max}} \frac{t_i^{\max} - t_i^{\min}}{t_{i+1}^{\min} - t_i^{\min}} \,, \tag{1}$$

where $N^{\max}$ is the total number of maxima. The breathing phase corresponding to each real-time scan, ϕ_j, was linearly interpolated as a function of its acquisition time t_j, using

$$\phi_j = \begin{cases} \left(\frac{t_j - t_i^{\min}}{t_i^{\max} - t_i^{\min}} \right) \bar{\phi}^{\max} & \text{for } t_i^{\min} \leq t_j < t_i^{\max} \\ \bar{\phi}^{\max} + \left(\frac{t_j - t_i^{\max}}{t_{i+1}^{\min} - t_i^{\max}} \right) (1 - \bar{\phi}^{\max}) & \text{for } t_i^{\max} \leq t_j < t_{i+1}^{\min} \end{cases} , \tag{2}$$

with $i = 1, ..., N^{\max}$ and $j = 1, ..., N^{\text{acq}}$.

2.4 Motion Model

With the method outlined in the previous section, each real-time scan was assigned a respiratory phase ϕ_i, which, together with the deformable registration results, gave a set of tissue displacements at each voxel location $\boldsymbol{r}$, denoted by

$$\boldsymbol{u}_i(\boldsymbol{r}) \equiv \boldsymbol{u}(\boldsymbol{r}, \phi_i) \,, \quad \text{with} \quad i = 1, \ldots, N^{\text{acq}} \,. \tag{3}$$

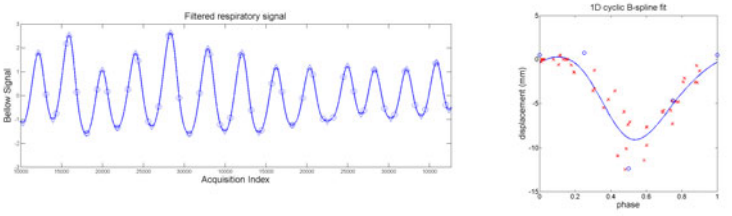

Fig. 2. Signal from a respiratory bellow (*left*) as a function of acquisition index illustrating variations in breathing amplitude. Open circles indicate the real-time MR acquisitions, whereas triangles indicate minima and maxima. B-spline fit to displacement data (*right*) as a function of phase at a single location in the liver. Open circles indicate the B-spline control points (i.e. the motion model coefficients).

To interpolate these displacement data, we used a 1-D cyclic homogeneous cubic B-spline with four control points as a fitting function, given by

$$\hat{\boldsymbol{u}}(\boldsymbol{r},\phi) = \sum_{k=1}^{k=4} f_k(\phi)\boldsymbol{\beta}_k(\boldsymbol{r}) \;, \tag{4}$$

where $f_k(\phi)$ are the B-spline basis functions, and $\boldsymbol{\beta}_k(\boldsymbol{r})$ are the control point values (i.e. the motion model coefficients) at each location $\boldsymbol{r}$ and for each spatial direction x, y, and z. This particular fitting function was chosen because previous work had shown it to give the best approximation to the registration results [13].

By substituting equation (3) into (4), we obtain a set of N^{acq} equations for the known displacements $\boldsymbol{u}_i$, given by

$$\begin{bmatrix} \boldsymbol{u}_1(\boldsymbol{r}) \\ \boldsymbol{u}_2(\boldsymbol{r}) \\ \vdots \\ \boldsymbol{u}_{N^{\mathrm{acq}}}(\boldsymbol{r}) \end{bmatrix} = \begin{bmatrix} f_1(\phi_1) & f_2(\phi_1) & f_3(\phi_1) & f_4(\phi_1) \\ f_1(\phi_2) & f_2(\phi_2) & f_3(\phi_2) & f_4(\phi_2) \\ \vdots & \vdots & \vdots & \vdots \\ f_1(\phi_{N^{\mathrm{acq}}}) & f_2(\phi_{N^{\mathrm{acq}}}) & f_3(\phi_{N^{\mathrm{acq}}}) & f_4(\phi_{N^{\mathrm{acq}}}) \end{bmatrix} \begin{bmatrix} \boldsymbol{\beta}_1(\boldsymbol{r}) \\ \boldsymbol{\beta}_2(\boldsymbol{r}) \\ \boldsymbol{\beta}_3(\boldsymbol{r}) \\ \boldsymbol{\beta}_4(\boldsymbol{r}) \end{bmatrix} . \tag{5}$$

From this over-determined system of linear equations, the unknown motion model coefficients $\boldsymbol{\beta}_k$ were found by computing the Moore-Penrose pseudo-inverse of the basis functions matrix $f_k(\phi_i)$ using singular value decomposition. Note that, since the basis functions are independent of $\boldsymbol{r}$, this inverse needs to be computed only once [3].

With the motion model coefficients known, equation (4) allows the computation of an approximate model displacement $\hat{\boldsymbol{u}}$ as a function of phase for every voxel location (Figure 2). Using the corresponding anatomical landmark points mentioned above, the mean target model error (TME), defined as the mean of the Euclidean distance between each landmark point in the reference volume and the corresponding locations predicted by the motion model for the other volumes, was computed for all volunteers.

2.5 Simulating Ultrasound Scan Lines

Synthetic ultrasound images were simulated using a fast propagation model similar to others described in the literature [5–8]. We assigned local impedance and absorption coefficients to different tissue types segmented from the breath-hold MR scan similar to [8], rather than using a conversion from CT Hounsfield units as in [5, 7].

Assuming a plane longitudinal acoustic wave propagating along a ray, and considering perpendicular reflection at a tissue interface i where the acoustic impedance changes from Z_{i-1} to Z_i, the ratio of reflected to incident intensity, $r_i^{\perp}$, is given by

$$r_i^{\perp} = \left(\frac{Z_i - Z_{i-1}}{Z_i + Z_{i-1}} \right)^2 \ , \tag{6}$$

with $i = 1, \ldots, N$, and boundary condition $r_1^{\perp} = 0$. Using a Lambertian reflection model, the intensity reflection ratio at an oblique interface can be written as

$$r_i = |\hat{\boldsymbol{x}} \cdot \hat{\boldsymbol{n}}_i| r_i^{\perp} = \frac{|\hat{\boldsymbol{x}} \cdot \nabla Z_i|}{\|\nabla Z_i\|} r_i^{\perp} \ , \tag{7}$$

with $\hat{\boldsymbol{x}}$ a unit vector along the ray direction, and $\hat{\boldsymbol{n}}_i$ the unit normal at the i-th interface. In practice, the inner product term is obtained by computing the gradient of the impedance, as indicated by the right-most term.

The ratio of transmitted to incident intensity up to the i-th interface is computed by tracing along each ray using

$$t_i = \prod_{j=1}^{j=i} \left(1 - r_j^{\perp}\right) \ , \tag{8}$$

whereas the ratio of absorbed to incident intensity can be written as

$$A_i = \prod_{j=1}^{j=i} \exp\left(-0.1 \ln(10) \alpha_j \Delta x\right) \ , \tag{9}$$

with Δx the distance between successive sampling points along the ray, and the local absorption coefficient α_i has the units of $\mathrm{dB\,cm^{-1}}$. Combining equations (7), (8) and (9), the reflected intensity from the i-th interface, received at the transducer, is given by

$$I_i^{\mathrm{refl}} = I_0 \, t_i^2 \, A_i^2 \, r_i \ , \tag{10}$$

where the transmission and absorption terms are squared since the ultrasound wave is assumed to travel along the same path twice. The effects of finite beam width in the elevational direction were simulated by convolving I_r along the beam direction with a Gaussian, while the effects of multiple active transducer elements was taken into account by convolving I_r perpendicular to the beam direction with a 1-D triangular window function [6, 8, 14].

To obtain realistic speckle patterns representative of liver parenchyma, we applied a texture quilting technique using real ultrasound images as input [15, 16],

as a computationally efficient alternative to performing extensive scattering simulations [6]. Inverse log-compression was applied to the texture map, resulting in a texture intensity I^{text}, which was blended with the reflected intensity (10) using

$$I^{\text{tot}} = w\, I^{\text{refl}} + (1 - w)\, t^2\, A^2\, I^{\text{text}} \,, \tag{11}$$

with blending weight w. The final log-compressed ultrasound scan line image was computed from

$$I^{\text{US}} = \log(1 + aI^{\text{tot}}) / \log(1 + a) \,, \tag{12}$$

where a is the log-compression factor.

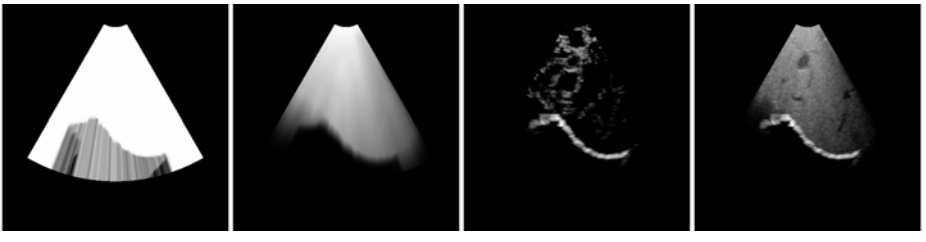

Fig. 3. Example of log-compressed simulated transmission, absorption, reflection, and final ultrasound B-mode image (*left-to-right*)

2.6 Simulating Dynamic B-Mode Ultrasound

To obtain 3-D impedance and absorption maps for the different tissues, we used semiautomatic methods to segment the breath-hold MR scan into liver, blood vessels, lung and ribs. The vessels were segmented using a Hessian-based multiscale filter [17]. Literature values for impedance and absorption coefficients were assigned to the segmented regions [18] (see Table 1), and Gaussian distributed noise was added to introduce small spatial inhomogeneities within regions of single tissue type.

Table 1. Acoustic impedance Z (in $10^6 \text{kg}\,\text{s}^{-1}\text{m}^{-2}$) and absorption coefficient α (in $\text{dB}\,\text{cm}^{-1}$) for tissue types considered in this study [18]

	liver	blood	lung	ribs
Z	1.65	1.61	0.50	7.8
α	0.94	0.18	12.0	20.0

To simulate a dynamic B-mode ultrasound sequence, we defined a sector-shaped region representing an ultrasound image at a location in the breath-hold MR volume (Fig. 4). The apical edge of this sector, representing the curvilinear ultrasound transducer face, was placed on the skin surface below the rib cage with the sector axis pointing upwards at an angle such that the liver, diaphragm,

and part of the right lung were in view (Fig. 4). Please note that probe induced liver deformations were not taken into account.

Values for motion model B-spline control point coefficients $\boldsymbol{\beta}$ were obtained at regularly spaced points across the sector using linear interpolation. Displacements of these points were computed using equation (4) resulting in a warped sector point-set. The impedance and absorption coefficients were linearly interpolated across the warped sector, and equation (12) was used to simulate a B-mode sector scan (Fig. 3). By varying the breathing phase and repeating the simulation, a dynamic sequence of B-mode scans was obtained.

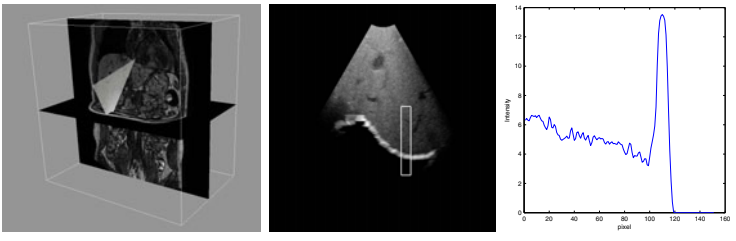

Fig. 4. Virtual ultrasound sector positioned inside the MR breath-hold volume (*left*), the resulting simulated B-mode image showing the diaphragm navigator window (*centre*), and the corresponding 1-D profile (*right*)

By combining a physics-based ultrasound propagation model with the texture maps our simulated ultrasound images contain sufficient characteristics of real ultrasound images, allowing acquisition of a breathing signal from the moving diaphragm, as explained in the next section.

2.7 Ultrasound Diaphragm Navigator Breathing Signal

Surrogate breathing signals were extracted from the simulated dynamic B-mode sequences by positioning a narrow navigator window at the diaphragm location [10] (see Fig. 4, centre image). By integrating across this navigator and computing the maximum of the resulting 1D profile (Fig. 4, right), a diaphragm navigator breathing signal s was obtained, which was normalised. This was done for both the tracked ultrasound and the synthetic ultrasound, resulting in the normalised signals s^{t} and s^{s}, respectively.

2.8 Synchronisation Accuracy: Motion Model Phase Error

The known relation $\phi(s^{\mathrm{s}})$ between the synthetic signal s^{s} and the motion model phase ϕ can be used to instantiate the motion model during an intervention using the signal s^{t} from the tracked ultrasound. In practice, spatial misalignments between the tracked and synthetic ultrasound result in differences between the signals s^{t} and s^{s}, leading to small errors in the phase ϕ at which the motion model is instantiated (Fig. 5). Since, in this study, we used a simulation to represent the

tracked ultrasound, the "ground-truth" relation $\phi(s^{\mathrm{t}})$ is also known. This allows quantifying the synchronisation accuracy by the following phase error metric:

$$\Delta\phi = \phi(s^{\mathrm{t}}) - \phi(s^{\mathrm{s}}) \; . \tag{13}$$

3 Results and Discussion

Numerical results for the target registration and target model error are given in Table 2. The mean liver displacement of 4.6 ± 3.8 mm before correction was reduced to 2.5 ± 1.7 mm when applying the motion model, which is comparable to the real-time MR scan voxel size (1.5 mm in plane, 4 mm out of plane).

Table 2. Mean, standard deviation, and maximum displacement in mm of the corresponding anatomical landmarks (second column). For each volunteer five landmarks at different locations throughout the liver were used. Residual displacements after registration correction (TRE, third column), and after motion model correction (TME), are given in the third and fourth columns, respectively.

	displacement			TRE			TME		
volunteer	mean	σ	max	mean	σ	max	mean	σ	max
1	4.7	3.3	16.3	2.2	1.1	6.0	2.4	1.3	7.7
2	4.6	4.3	17.4	2.3	1.6	7.2	2.6	1.9	10.2
3	4.4	3.7	20.9	2.1	1.4	12.4	2.4	1.7	14.6
all	4.6	3.8	20.9	2.2	1.4	12.4	2.5	1.7	14.6

Deformable registration of a single real-time scan took around 30 minutes on a standard PC. To speed up the non-rigid registrations we are preparing to use a GPU accelerated registration method [19], and initial tests showed a computation time of approx. 60 seconds per registration.

The time needed to calculate the motion model coefficients $\boldsymbol{\beta}(\boldsymbol{r})$ across the complete volume by inverting equation (5) was approx. 2 minutes. Reslicing and interpolating the coefficients and simulating a single ultrasound image took of the order of a few seconds. Since we would eventually like to use our technique in clinical applications, real-time simulation of the synthetic ultrasound will be required, which can potentially be achieved using GPU techniques [6, 7].

Fig. 5 shows plots of the navigator signals and resulting phase error (13) due to translations along the superior-inferior axis of ± 2 cm of the tracked ultrasound with respect to the synthetic ultrasound, which represents an estimate of the upper limit of misalignment one may expect at the start of a treatment. The resulting maximum phase error was approx. 3 %, which indicates that the phase error is rather insensitive to alignment inaccuracies. This could potentially also be of importance for applications where the location of a diaphragm navigator used during pre-operative imaging is different from the location used during intervention [4].

Finally, comparing the tracked ultrasound signal directly to the bellow signal could be an alternative and more direct way for synchronising the motion

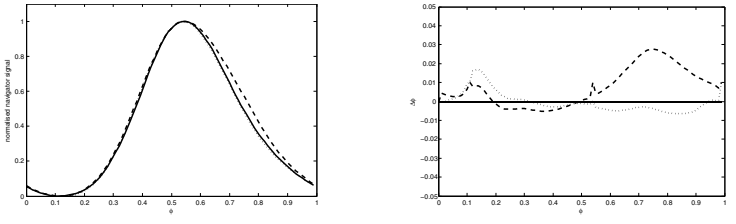

Fig. 5. Navigator signals (*left panel*) for the tracked (*solid line*) and synthetic ultrasound for misalignments in the superior-inferior direction of +2 cm (*dashed line*) and −2 cm (*dotted line*). Corresponding phase error $\Delta\phi$ (*right panel*) as a function of motion model input phase ϕ.

model to a subject's breathing. However, since these signals would potentially capture different breathing modes, like chest and abdominal breathing, a larger synchronisation error may result.

4 Conclusion

We presented a method for building a realistic liver motion model from MR scans obtained during breath-hold and real-time breathing. Applying the motion model to the segmented breath-hold volume, and using a fast ultrasound propagation model, dynamic B-mode sequences were simulated. A surrogate breathing signal was then computed by positioning a navigator window across the diaphragm, from which a motion model phase error, due to spatial misalignment between tracked ultrasound and synthetic ultrasound, was obtained. We found that for spatial misalignments of ±2 cm, the maximum phase error was approx. 3 %, indicating that synchronising a motion model to a subject's breathing is rather insensitive to inaccuracies in tracked ultrasound localisation.

Acknowledgments. We would like to thank Tobias Schaeffter for his help in acquiring the MR data, and Jamie McClelland for advice on motion models. This work was funded by EPSRC grant EP/F025750/1, and a UCL/UCLH Comprehensive Biomedical Research Centre (CBRC) grant (No. 96). Dean Barratt is funded by the Royal Academy of Engineering Research Fellowship scheme.

References

1. McClelland, J.R., Blackall, J.M., Tarte, S., et al.: A continuous 4D motion model from multiple respiratory cycles for use in lung radiotherapy. Medical Physics 33(9), 3348–3358 (2006)
2. Nguyen, T.N., Moseley, J.L., Dawson, L.A., et al.: Adapting liver motion models using a navigator channel technique. Medical Physics 36(4), 1061–1073 (2009)
3. White, M.J., Hawkes, D.J., Melbourne, A., et al.: Motion artifact correction in free-breathing abdominal MRI using overlapping partial samples to recover image deformations. Magnetic Resonance in Medicine 62(2), 440–449 (2009)

4. King, A.P., Boubertakh, R., Rhode, K.S., et al.: A subject-specific technique for respiratory motion correction in image-guided cardiac catheterisation procedures. Medical Image Analysis 13(3), 419–431 (2009)
5. Wein, W., Brunke, S., Khamene, A., et al.: Automatic CT-ultrasound registration for diagnostic imaging and image-guided intervention. Medical Image Analysis 12(5), 577–585 (2008)
6. Shams, R., Hartley, R., Navab, N.: Real-time simulation of medical ultrasound from CT images. In: Metaxas, D., Axel, L., Fichtinger, G., Székely, G. (eds.) MICCAI 2008, Part II. LNCS, vol. 5242, pp. 734–741. Springer, Heidelberg (2008)
7. Reichl, T., Passenger, J., Acosta, O., Salvado, O.: Ultrasound goes GPU: real-time simulation using CUDA. In: SPIE, vol. 7261 (2009)
8. King, A.P., Ma, Y.-L., Yao, C., Jansen, C., Razavi, R., Rhode, K.S., Penney, G.P.: Image-to-physical registration for image-guided interventions using 3-D ultrasound and an ultrasound imaging model. In: Prince, J.L., Pham, D.L., Myers, K.J. (eds.) IPMI 2009. LNCS, vol. 5636, pp. 188–201. Springer, Heidelberg (2009)
9. Ruan, D., Fessler, J.A., Balter, J.M., Keall, P.J.: Real-time profiling of respiratory motion: baseline drift, frequency variation and fundamental pattern change. Physics in Medicine and Biology 54(15), 4777–4792 (2009)
10. Timinger, H., Krueger, S., Dietmayer, K., Borgert, J.: Motion compensated coronary interventional navigation by means of diaphragm tracking and elastic motion models. Physics in Medicine and Biology 50(3), 491–503 (2005)
11. Crum, W.R., Tanner, C., Hawkes, D.J.: Anisotropic multi-scale fluid registration: evaluation in magnetic resonance breast imaging. Physics in Medicine and Biology 50(21), 5153–5174 (2005)
12. von Siebenthal, M., Székely, G., Lomax, A.J., Cattin, P.C.: Systematic errors in respiratory gating due to intrafraction deformations of the liver. Medical Physics 34(9), 3620–3629 (2007)
13. McClelland, J.R., Chandler, A.G., Blackall, J.M., Ahmad, S., Landau, D.B., Hawkes, D.J.: 4D motion models over the respiratory cycle for use in lung cancer radiotherapy planning. In: SPIE, vol. 5744, pp. 173–183 (2005)
14. Goldstein, A., Madrazo, B.L.: Slice-thickness artifacts in gray-scale ultrasound. Journal of Clinical Ultrasound 9(7), 365–375 (1981)
15. Efros, A.A., Freeman, W.T.: Image quilting for texture synthesis and transfer. In: SIGGRAPH 2001, pp. 341–346. ACM, New York (2001)
16. Zhu, Y., Magee, D.R., Ratnalingam, R., Kessel, D.: A virtual ultrasound imaging system for the simulation of ultrasound-guided needle insertion procedures. In: Medical Image Understanding and Analysis (2006)
17. Frangi, A., Niessen, W., Vincken, K., Viergever, M.: Multiscale vessel enhancement filtering. In: Wells, W.M., Colchester, A.C.F., Delp, S.L. (eds.) MICCAI 1998. LNCS, vol. 1496, pp. 130–137. Springer, Heidelberg (1998)
18. Curry, T.S., Dowdey, J.E., Murry, R.C.: Christensen's Physics of Diagnostic Radiology, 4th edn. Lea & Febiger, Philadelphia (1990)
19. Modat, M., Ridgway, G., Taylor, Z., et al.: Fast free-form deformation using graphics processing units. In: Computer Methods and Programs in Biomedicine (2009)